Cycle structures for retinal image registration

Anonymous ACCV 2014 submission

Paper ID 669

Abstract. This paper presents a novel cycle structural feature for retinal image registration. The cycle structures are composed of several bifurcation points, intersection points of arteries or veins and the vessels connected with them. They are stable visual features and can be used as features for registration. In order to find the independent cycles efficiently, we develop a new dynamic path moving algorithm. The characteristic vectors used to describe them consist of the normalized branch angles and lengths, which are invariant against translation and rotation. A matching process based on the characteristic vectors is operated to find best matching pairs to estimate the parameters of affine transformation for registration. This method can greatly reduce the wrong matching pairs that may generate in the single bifurcation point matching. Compared to the bifurcation structures [1], more branch angles and lengths are taken into account which make the cycle structures more unique and stable. Moreover, our method avoids the unaligned problems caused by concentration and overlapping of best matching pairs. Experimental results show that this algorithm is feasible and effective for registration.

1 Introduction

Retinal images contain valuable local and time information as they can be taken at different time or with different perspectives. Retinal image registration can integrate some local and time information from different images into one image according to their characteristics, which is a key technology to help ophthalmologists to analyze and diagnose various diseases comprehensively. In this paper, we focus on the issue of integrating the information of two retinal images into one image. Toward this goal, a novel feature-based retinal image registration method based on cycle structures is proposed.

During the past decades, many methods for retinal image registration have been proposed, which can be grouped into two categories: intensity-based methods and feature-based methods [2]. The calculation processes of intensity-based algorithms are usually complicated as they need to integrate the whole image information to calculate the similarity measure [3–5]. They generally optimize an objective function based on comparison of intensities or intensity gradients [6], or rely on measures such as mutual information [7]. The reliability of these methods mainly depends on the original image, which means that large intensity variances or poor quality images may make them invalid.

Feature-based methods mainly rely on the shape characteristics of retina such as vessels, bifurcation points and intersection points. In [8], the branch angles

of each bifurcation point were used to produce a probability for two points to match. Stewart et al. [9] proposed dual-bootstrap iterative closest point (Dual-Bootstrap ICP) algorithm to extract vessel bifurcations and found 12-parameter quadratic transformations between two images by means of an iterative process. In [10], the centerlines of the tubular objects were extracted and the multiscale heuristics and optimal-scale measures were presented to minimize the effects of noise and singularities. Chanwimaluang et al. [11] extracted the vascular tree by using an efficient local entropy-based thresholding technique. Perez-Rovira et al. [12] treated the bifurcation points and vessel segments as features and used them to warp for registration respectively. However, these methods largely depend on the branch angles of single bifurcation point, and these angles are hard to calculate precisely which may lead to the mismatch of registration.

Chen [1] presented a bifurcation structure to overcome the mismatch problem caused by the point-matching methods. The bifurcation structure consists of a master bifurcation point and its three connected neighbors. Branch angles and lengths form 15-dimensional characteristic vectors which can reduce the probability of mismatch. However, the detected best matching pairs used to estimate the parameters of affine transformation usually concentrate together and partially overlap, which make the vessels that far away from the matching pairs not well aligned. Moreover, advanced imaging devices and state of the art segmentation methods can produce more and more complicated vascular trees that may confuse the matching of bifurcation structures and fail on registration.

In view of this, we propose a new cycle structure for feature-based retinal image registration shown in Fig. 1. Considering the fact that the bifurcation points and intersection points of arteries or veins can make up cycles [13] which can't change no matter how the visual angle changes, we build the cycle structures which are stable visual features and can be used for registration. A cycle structure is composed of several bifurcation points, intersection points of arteries or veins and the vessels connected with them. The characteristic vector of each structure is composed of the normalized branch angles and lengths which are invariant against translation and rotation. A matching process based on the characteristic vectors is operated to find the best matching pairs used to estimate the parameters of affine transformation for registration. Compared to the bifurcation structures [1], more branch angles and lengths are taken into account which make the cycle structures more unique and stable for registration. Moreover, the detected best matching pairs are relatively independent which avoid the unaligned problems caused by concentration and overlapping of best matching pairs. Experimental results show that our method is feasible and effective for registration purpose.

2 Segmentation and skeleton

Due to hardware limitations, retinal images usually have characteristics of uneven illumination, large numbers of noise points and low contrast between vessels

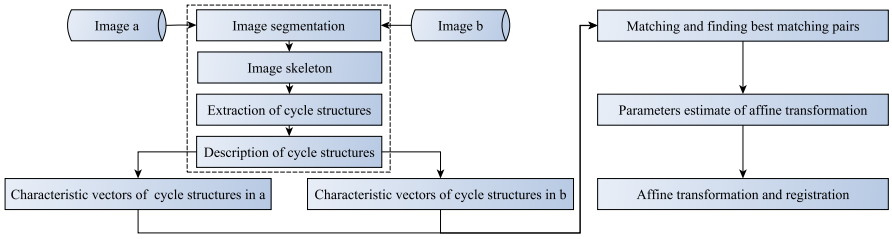

Fig. 1. Registration algorithm base on cycle features.

and background, which lead to the challenge of automatic analysis. The result of retinal image segmentation plays a key role on the accuracy of registration.

Multiwavelet kernels and multiscale hierarchical decomposition method [14] are adopted for retinal image segmentation in our work. This method first enhances the vessels using matched filtering with multiwavelet kernels, separating vessels from clutter and bright, localized features. And the noise removal and vessel localization are achieved by a multiscale hierarchical decomposition of the normalized enhanced image. Then a necessary condition is set to achieve the optimal decomposition and derive the associated value of the scale parameter controlling the amount of details captured. Finally, a binary map of the vasculature is obtained by locally adaptive thresholding. This segmentation method demonstrates excellent performance in DRIVE and STARE standard retinal datasets.

In order to obtain the binary image with one pixel width vascular tree, we use the skeleton program provided by Nicholas [15] which is intuitive and noise-resistant. It can be seen from the examples shown in Fig. 2 that the segmentation and skeleton results are still acceptable and available even if the images are low contrast.

3 Cycle structures

3.1 Extraction

A cycle structure is composed of several bifurcation points, intersection points of arteries or veins and the vessels connected with them. The extraction procedure of cycle structures can be implemented by three steps: detecting feature points, filtering feature points and finding cycle structures.

Detecting feature points Bifurcation points and intersection points are significant feature points of the vascular tree structure. The feature point is determined by the 8-adjacent pixels of one pixel. In general, we treat the pixel whose value is equal to 1 in binary image with three and four adjacent pixels in the same value as three-bifurcation feature point (Fig. 3(a)) and four-bifurcation

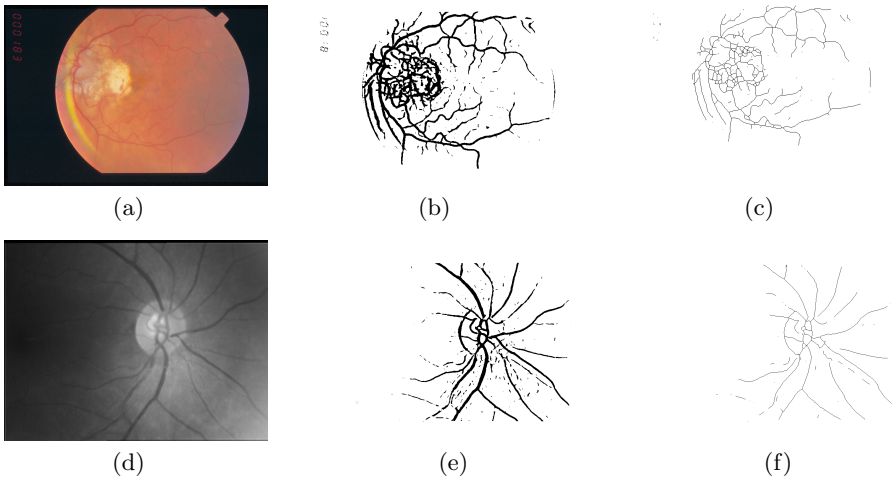

(a) (b) (c)

(d) (e) (f)

Fig. 2. Segmentation and skeleton on low contrast retinal images. (a) and (d) are original images. (b), (e) and (c), (f) are the corresponding segmentation and skeleton results, respectively.

feature point (Fig. 3(b)) respectively. After all the feature points are found, each feature point is considered as the seed for searching the feature points connected to it along the blood vessels. Then all the feature points with their connectivities are detected.

1	0	0	1	0
0	1	0	1	0
0	0	1	0	0
0	0	1	0	0
0	0	1	0	0

(a)

0	0	1	0	1
0	0	1	1	0
1	1	1	0	0
0	0	1	0	0
0	0	1	0	0

(b)

Fig. 3. Feature points. The red pixels in the center are three-bifurcation feature point and four-bifurcation point respectively.

The concept of feature points and connectivities can be extended from the field of graph theory. A graph can be represented by a pair of set (V, E), where V is the set of vertices and E is the set of edges [16], and the feature points can

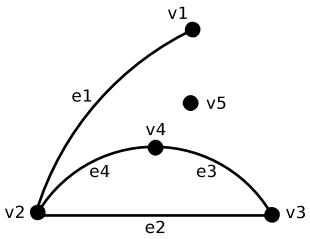

Fig. 4. Vertices and edges in a graph. $v_1 \sim v_5$ and $e_1 \sim e_4$ represent vertices and edges respectively.

be treated as vertices while their connectivities can be treated as edges. The connectivities can be explained by the node-edge adjacent structure in graph theory as it lists adjacent vertices for each vertex. Fig. 4 shows the graph composed of vertices $v_1 \sim v_5$ and edges $e_1 \sim e_4$. The node-edge adjacent structure in Fig. 4 is shown in Table 1. The first column represents all vertices while the remaining columns list the corresponding adjacent vertices.

Table 1. Node-edge adjacent structure. The first column represents all vertices and the rest columns list the corresponding adjacent vertices.

Vertex	Adjacent vertices		
v_1	v_2	0	0
v_2	v_1	v_3	v_4
v_3	v_2	v_4	0
v_4	v_2	v_3	0
v_5	0	0	0

Filtering feature points The complicated vessel structures and the connectivities can be greatly simplified by removing the invalid feature points. As is known, the condition that a vertex belongs to a cycle is that it must have at least two adjacent vertices. In other words, this vertex should appear at least three times in the node-edge adjacent structure. Thus, the invalid vertices can be filtered according to this rule. Fig. 5(a) and Fig. 5(b) give all detected feature points and the remaining feature points after filtering respectively. The number of target vertices is reduced from 211 to 164 which greatly improves the efficiency and reduces the complexity of the algorithm. If the vessels in the retinal images are complicated, the bifurcation structures [1] may become confused because of the existing invalid feature points.

Finding cycle structures Finding cycle structures in retinal image is a challenging task as the vascular trees are complicated. Learning from graph theory,

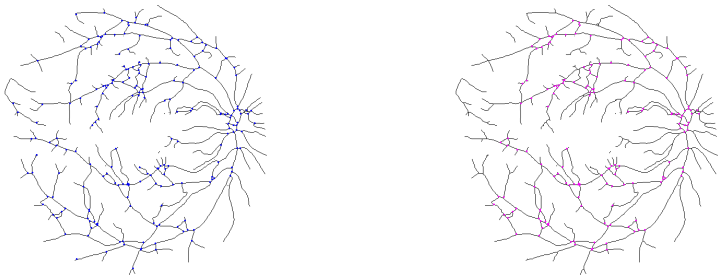

(a) (b)

Fig. 5. All detected feature points (a) and the remaining feature points (b) after filtering.

we address the problem of finding cycle structures in image to that of finding cycles in graph [17].

There are many algorithms proposed to find the cycles in graph theory. However, most of them focus on finding all connected cycles rather than independent cycles which are not available for our purpose. An independent cycle consists of the fewest vertices starting and ending at the same vertex without any other cycles included in it. In order to find the independent cycles efficiently and accurately, we develop a new dynamic path moving algorithm to improve the method presented in [17]. The main idea of the algorithm is to transform the node-edge adjacent structure into a tree structure that can be used to find the cycle structures.

The dynamic path moving algorithm can be summarized as follows:

1. Initialize a vertex as the predecessor of the tree structure.
2. Find the adjacent vertices of the predecessor and treat them as the first descendants of the predecessor. The adjacent vertices can be found according to the filtered node-edge adjacent structure as it lists all the vertices adjacent to one vertex.
3. Continue to find the adjacent vertices of the first descendants and treat them as the second descendants. It is worth noting that, the relationship of predecessor and descendants can't be contrary. In other words, once one vertex v_a is considered as the predecessor of the other vertex v_b, v_b can't be the descendant of v_a any more.
4. Determine whether there is a vertex in the current three layers appearing twice in the tree structure. The appearance of such a vertex marks the formation of a cycle structure. This vertex and its predecessors in the front two layers will be exported as they are seen as members that can consist of a cycle. Then this vertex will be treated as an ending point and we will not find its adjacent vertices anymore.

5. Determine whether there is a vertex not being an ending point in current layer. This kind of vertices is needed continue to find its adjacent vertices and treated as the next layer in the tree.
6. Repeat the steps 4 and 5 until all the vertices in current layer are ending points.

All the cycle structures can be found by the above steps. Then the Dijkstra algorithm [18] is used to check that whether the cycle structure is independent. It treats the starting points as the center point and extends outward layer by layer until extending to the ending point in the cycle structure. Through this step, the unavailable cycle structures are removed and cycle structures are finalized eventually.

Fig. 6(a) can be transformed into tree structure in Fig. 6(b) by using the rules above. Adjacent vertices of each vertex in Fig. 6(b) are founded according to the filtered node-edge adjacent structure shown in Table 2. Vertices v_5, v_6, v_7 in Fig. 6(b) is treated as ending points as they appear twice in the first three layers. So the cycle structures composed of $v_1v_5v_6$ and $v_1v_6v_7v_8$ can be exported. Vertices v_3 and v_4 need continue to find their adjacent vertices as they are not the ending points. We totally find three cycle structures in the end. Vertices $v_1v_5v_6$ consist of three-point cycle, $v_1v_6v_7v_8$ consist of four-point cycle and $v_1v_2v_3v_4v_5$ consist of five-point cycle. The shortest path algorithm is used then to check that whether the cycle is independent, for example, a connected cycle which is composed of vertices $v_1v_5v_6v_7v_8$ is removed.

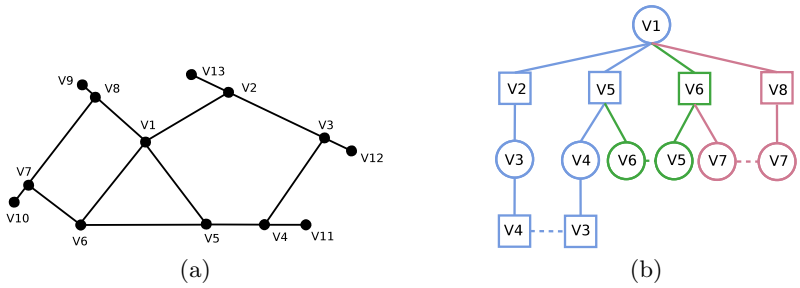

Fig. 6. Cycle structures and the transformed tree. From (b), we can obtain that vertices $v_1v_5v_6$ consist of three-point cycle, $v_1v_6v_7v_8$ consist of four-point cycle and $v_1v_2v_3v_4v_5$ consist of five-point cycle.

3.2 Description

Most feature-based retinal image registration methods use bifurcation points or intersection points as the feature points because they are prominent visual features that can be recognized by their branches. However, the calculated branch

Table 2. The filtered node-edge adjacent structure of Fig. 6(a). Adjacent vertices of each vertex in Fig. 6(b) are founded according to this structure.

Vertex	Adjacent vertices			
v_1	v_2	v_5	v_6	v_8
v_2	v_1	v_3	0	0
v_3	v_2	v_4	0	0
v_4	v_3	v_5	0	0
v_5	v_1	v_4	v_6	0
v_6	v_1	v_5	v_7	0
v_7	v_6	v_8	0	0
v_8	v_1	v_7	0	0

angles may be imprecisely which leads to the nonuniqueness of the feature points. It is easy to generate mismatch due to this reason. Bifurcation structures [1] have integrate four connected bifurcations into one structure. The increased angles and lengths are composed of 15-dimensional characteristic vectors which can reduce the probability of mismatch.

In this paper, cycle structures are presented. The feature points composed of cycle structure have more angle and length information which makes the cycle structure become more unique.

The factors used to describe cycle structures are shown in Fig. 7. The cycle structure can be described by the branch lengths $L_1 \sim L_4$, branch angles $\theta_1 \sim \theta_{14}$ and angles between feature points $\theta_{15}\theta L_{18}$. Branch lengths are calculated via Euclidean distance while angles between feature points are calculated via the location of feature points. The branch angles are calculated as follows. The feature point is treated as a center pixel firstly and a $7 * 7$ pixel area is chosen to applied to it. Then the branch angles are obtained by calculating the angles between boundary pixel whose pixel value is 1 and the center pixel. In this way, branch angles are divided into 24 directions while each direction has 15°. After all the angles and lengths being calculated, the characteristic vectors can be obtained by formula (1). As normalized lengths and angles can be invariant to translation and rotation, a normalization process is utilized by formula (2) and (3). L_i and θ_i represent the i-th branch length and angle respectively.

$$\begin{aligned}\tilde{v} = \{length, angles\} = \{L_1, L_2, L_3, L_4, \theta_1, \theta_2, \theta_3, 0, \theta_4,\\ \theta_5, \theta_6, \theta_7, \theta_8, \theta_9, \theta_{10}, \theta_{11}, \theta_{12}, \theta_{13}, \theta_{14}, 0, \theta_{15}, \theta_{16}, \theta_{17}, \theta_{18}\}\end{aligned} \tag{1}$$

$$L_i = \frac{L_i}{L_1 + L_2 + L_3 + L_4} \tag{2}$$

$$\theta_i = \frac{\theta_i}{360^\circ} \tag{3}$$

It is worth mentioning that, the number of feature points which can compose of a cycle structure is different which leads to a variation in length of the

characteristic vectors. Considering most of the feature points have three or four angles, we set four angles as standard. The last angle will be determined as zero if a feature point has three angles.

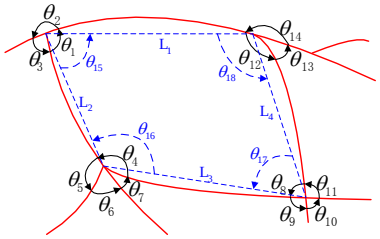

Fig. 7. Lengths and angles in cycle structure. $L_1 \sim L_4$, $\theta_1 \sim \theta_{14}$ and $\theta_{15} \sim \theta_{18}$ represent branch lengths, branch angles and angles between feature points respectively.

3.3 Matching and transformation

The feature matching process will search good similarity among all structure pairs. Assume that the i-th cycle structure of one image is expressed as V_i and the j-th cycle structure of the correspondence image is denoted as W_j, the similarity of the two structure pairs can be calculated by formula (4). m and n are the numbers of the cycle structures in these two images respectively. The S_{ij} denotes the distance between the pairs as similarity measure. The smaller the value, the better the similarity.

$$S_{ij} = sum|V_i - W_j| \qquad i = 1, 2 \ldots m; j = 1, 2 \ldots n \tag{4}$$

As we known above, the length of characteristic vector is different as the number of feature points composed of cycle is unequal. Characteristic vector's length of three-point cycle, four-point cycle and five-point cycle is 18, 24 and 30 respectively. Similarity measure will be calculated among structures composed of same number of vertices. Each kind of structures has a minimum similarity measure which means that three best matching pairs is detected. A threshold value is set to make sure that these three matching pairs are correct match.

It is well known that the affine transformation needs at least 3 pairs of points to transform. As cycle structure formed requires three points at least, one structure pair is enough to estimate the parameters for transformation. More points can ensure the accuracy of transformation. The transformation estimation can be calculated by formula (5).

$$e_{(pq,st)} = mean((M(v_p, w_q) - M(v_s, w_t))^2) \tag{5}$$

Here $M(v_p, w_q)$ and $M(v_s, w_t)$ are the transformation models estimated from the matched pairs v_p and w_q, v_s and w_t respectively. These two pairs must have good similarity by calculating the formula (4). Through this step, the best transformation parameters which can reduce the mismatch as much as possible is obtained. One image will be transformed to the other according to these parameters and the registration result is obtained.

4 Experiments and discussion

To the best of our knowledge, there exist rare public datasets of retina images for registration purpose. Therefore, we evaluate the proposed approach on the images acquired from Prof. Stewarts group at Rensselaer Polytechnic Institute and VARIA database [19] with a set of retinal images published for authentication purpose. The database currently includes 233 images from 139 different individuals, among which 59 groups contain different images from the same individual. However, only 10 groups are chosen for registration because there exist translation and rotation of captured retina in different images which is easy to evaluate the experimental results.

We first segment the images by multiwavelet kernels and multiscale hierarchical decomposition method [14] and skeletonize the vascular trees by [15]. Then we find all the cycle structures in each image and describe them as characteristic vectors. Finally, a matching process is operated to find the best matching pairs to estimate the parameters of affine transformation for registration. Fig. 1 shows the procedure.

In order to reduce the complexity of the algorithm, we only extract the cycles composed of three points, four points and five points. Experiments validate that these cycles are enough for successful registration. Fig. 8(a) and Fig. 8(b) show a pair of retinal images taken at different times, and the corresponding skeleton vascular trees are shown in Fig. 8(d) and Fig. 8(e), in which 41 and 29 cycle structures are detected, respectively. The two matching pairs of cycle structures highlighted in Fig. 8(d) and Fig. 8(e) are chosen to estimate the parameters of affine transformation. The final registration result of the original retinal images and its matched vascular trees are shown in Fig. 8(c) and Fig. 8(f) respectively. It is observed that most of the vessels are aligned well.

In contrast, the point-matching method detects 170 and 156 points respectively in this pair of images. There will be 26520 matching pairs as similarity is calculated between every two points, from which we find that the similarity measure of 399 pairs is 0 because the branch angles are really similar and also calculated imprecisely. Therefore, it will be confused to execute the matching for registration, which means that the point-matching method may need to consider further constraints such as vessel location or width for feasible and effective registration. Moreover, the bifurcation structure matching method detects 136 and 114 bifurcation structures respectively and four pairs highlighted in Fig. 8(g) and Fig. 8(h) are chosen to estimate the parameters for affine transformation, and the registration result is shown in Fig. 8(i). Compared to this method, our

method can detect less structures and choose less matching pairs but obtain the similar registration result.

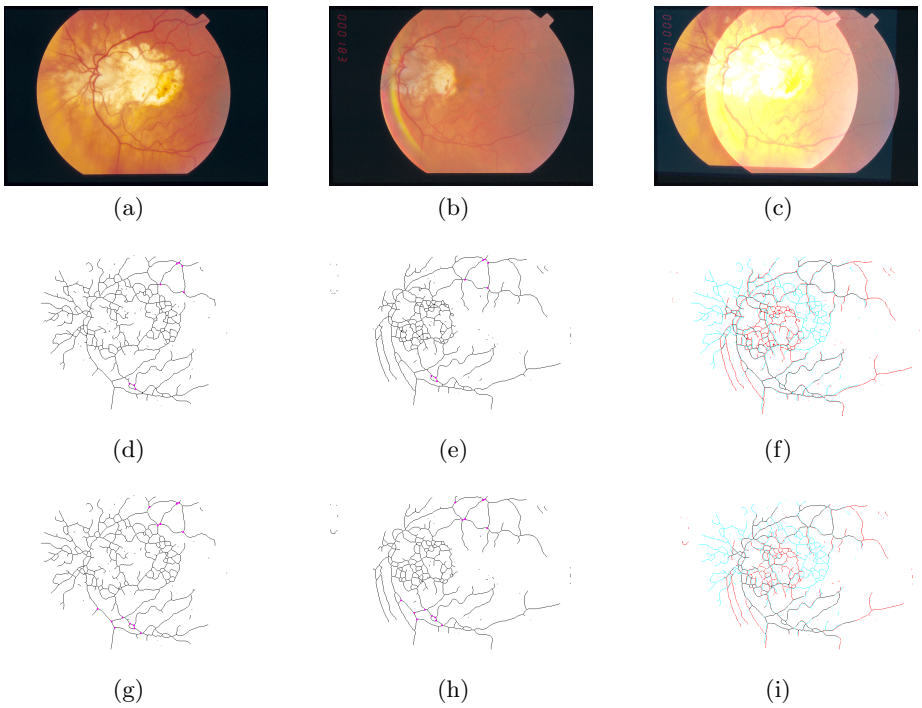

Fig. 8. The registration results on two retinal images. (a) and (b) are original retinal images acquired from Prof. Stewarts group at Rensselaer Polytechnic Institute. (c) is the registration result of our method. (f) is the corresponding matched vascular trees. The highlighted cycle structures in (d) and (e) are the best matching pairs used to estimate affine transformation parameters. (i) is the registration result of the registration method based on bifurcation structures. (g) and (h) are the corresponding best matching bifurcation structure pairs.

Experiments are also applied to the VARIA images such as Fig. 9(a) and Fig. 9(d) as one group of image pair chosen for registration. It can be seen that these two images have the characteristics of low contrast, big noise and less cycle structures which increase the difficulty of the registration. Only 6 and 10 cycle structures are detected in this case. However, our proposed method performs well on registration as shown in Fig. 9(b) and Fig. 9(e). Contrastly, 28 and 23 structures are detected by the bifurcation structure matching method and the registration result is not good as shown in Fig. 9(c) and Fig. 9(f) because the best matching pairs concentrate together and partially overlap which make the vessels far away from these pairs not well aligned as illustrated in Fig. 10.

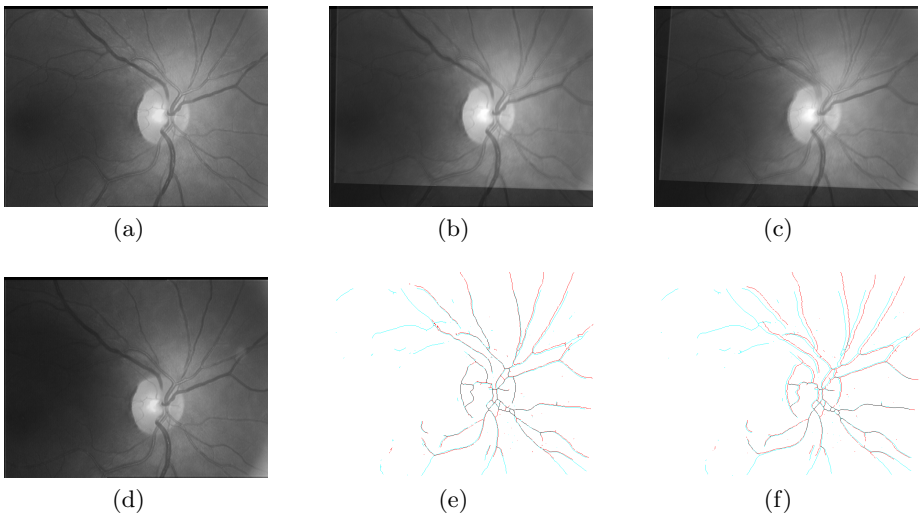

Fig. 9. The registration results on the images in VARIA database. (a) and (d) are original images. (b) and (c) are registration results obtained via our method and method based on bifurcation structures. (e) and (f) are corresponding vascular trees.

The results of the chosen 10 image pairs from VARIA database are shown in Table 3, which indicate that our method achieves better registration than the method based on bifurcation structures by avoiding the unaligned situations. However, our proposed method still mismatched in three situations that have less cycle structures than the others. By observing the original retinal images, it can be seen that these three pairs of images actually do not have many cycle structures.

5 Conclusion

To overcome the mismatch and unaligned problems, a feature-based retinal image registration method based on cycle structure is presented. The cycle structure is composed of bifurcation points, intersection points of arteries or veins and the vessels connected with them. It is invariant against translation and rotation. Experimental results validate that our proposed method is feasible and effective for registration purpose. Although our proposed method outperforms the previous methods on retinal image registration more precisely and robustly, it still need more effort to develop better segmentation method for exact vascular trees used to extract cycle structures in the future.

References

1. Chen, L., Xiang, Y., Chen, Y.: Retinal image registration using bifurcation structures. In: IEEE Internatinal Conference on Image Processing. (2011) 2169–2172

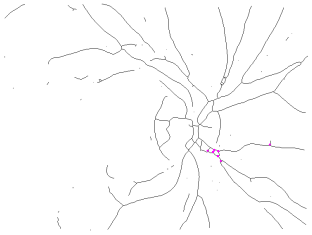

Fig. 10. Best matching pairs used for affine transformation (Concentration and overlaping problem of best matching pairs).

Table 3. Comparison results with VARIA database.

No.	Cycle structures			Bifurcation structures		
	Quantity		Registration result	Quantity		Registration result
	Image 1	Image 2		Image 1	Image 2	
1	4	14	mismatch	28	53	mismatch
2	12	12	success	55	49	unaligned
3	8	6	success	28	23	unaligned
4	10	6	success	50	27	mismatch
5	9	17	success	42	86	mismatch
6	17	14	success	66	45	success
7	6	10	success	39	39	success
8	1	5	mismatch	25	40	success
9	11	13	success	45	51	success
10	14	5	mismatch	69	30	unaligned

2. Zheng, J., Tian, J.: Salient feature region: A new method for retinal image registration. IEEE Transactions on Information Technology in Biomedicine **15** (2011) 221–232
3. Glocker, B., Komodakis, N., Paragios, N.: Inter and intra-modal deformable registration: Continuous deformations meet efficient optimal linear programming. In: Information Processing in Medical Imaging. (2007) 408–420
4. Nunes, J.C., Bouaoune, Y., Delechelle, E.: A multiscale elastic registration scheme for retinal angiograms. Computer Vision and Image Understanding **95** (2004) 129–149
5. Dreo, J., Nunes, J., Siarry, P.: Robust rigid registration of retinal angiograms through optimization. Computerized Medical Imaging and Graphics **30** (2006) 453–463
6. Penny, G.P., Weese, J.: A comparison of similarity measures for use in 2-d-3-d medical image registration. IEEE Transactions on Medical Imaging **17** (1998) 586–595
7. Maes, F., Collignon, A., Vandermeulen, D.: Multimodality image registration by maximization of mutual information. IEEE Transactions on Medical Imaging **16** (1997) 187–198
8. Zana, F., Klein, J.C.: A multimodal registration algorithm of eye fundus images using vessels detection and hough transform. IEEE Transactions on Medical Imaging **18** (1999) 419–428

9. Stewart, C.V., Tsai, C., Roysam, B.: The dual-bootstrap iterative closest point algorithm with application to retinal image registration. IEEE Transactions on Medical Imaging **22** (2003) 1379–1394
10. Aylward, S.R., Bullitt, E.: Initialization, noise, singularities, and scale in height ridge traversal for tubular object centerline extraction. IEEE Transactions on Medical Imaging **21** (2002) 61–75
11. Chanwimaluang, T., Fan, G., Fransen, S.R.: Hybrid retinal image registration. IEEE Transactions on Information Technology in Biomedicine **10** (2006) 129–142
12. Perez-Rovira, A., Cabido, R., Trucco, E.: Rerbee: robust efficient registration via bifurcations and elongated element applied to retinal fluorescein angiogram sequences. IEEE Transactions on Medical Imaging **31** (2012) 140–150
13. Kondermann, C., Kondermann, D., Yan, M.: Blood vessel classification into arteries and veins in retinal images. In: Medical Imaging: International Society for Optics and Photonics. (2007) 651247
14. Wang, Y., Ji, G., Lin, P.: Retinal vessel segmentation using multiwavelet kernels and multiscale hierachical decomposition. Pattern Recognition **46** (2013) 2117–2133
15. Nicholas, R.H.: Skeleton program (2006) http://cs.smith.edu/ nhowe/research/code/.
16. Bondy, Murty: Graph theory with applications. The Macmillan Press Ltd. (1976)
17. Jou, M.J., Chang, G.J.: The number of maximum independent sets in graphs. Taiwanese Journal of Mathematics **4** (2000) 685–695
18. Johnson, D.B.: A note on dijkstra's shortest path algorithm. Journal of Alternative and Complementary Medicine **20** (1973) 385–388
19. Ortega, M., Penedo, M.G., Rouco, J., Barreira, N., Carreira, M.J.: Personal verification based on extraction and characterization of retinal feature points. Journal of Visual Languages and Computing **20** (2009) 80–90